

# Dynamic response of a fractured excavation to blast and seismic waves

P.-C. Xu

*Consultant, Mississauga, Ontario, Canada*

J. O. Parra & C. L. Hackert

*Southwest Research Institute, San Antonio, Texas, U. S. A.*

**ABSTRACT:** In order to assess the strength, integrity and stability of a fractured underground excavation subjected to seismic and blast waves, a dynamic analysis of the displacement and stress fields around the excavation is carried out using a boundary integral equation (BIE) approach with a slip model of fracture. This paper outlines the approach and presents results of preliminary parametric studies. The results indicate that an intersecting fracture redistributes and usually amplifies the stress along and around the surface of the cavity. For certain combinations of the parameters, the stress amplification and complication can be very significant. It is found that the strongest stress concentration and deformation do not occur when the traction on the fracture is free but occur when the frequency dependent normalized slip stiffness parameters are of moderate values.

## 1. INTRODUCTION

An underground excavation such as tunnel, mine opening or permanent geological repository for nuclear wastes in a rock mass has to deal with the presence of prominent joints or joint sets or faults. The strength, integrity and stability of the excavation depend significantly on the characteristics of the fracture pattern as well as its strength and stiffness properties. In particular, the response of an excavation subjected to dynamic events such as earthquakes, underground explosions, blasts, or rock bursts can be critically controlled by nearby fractures in the rock. The dynamic interaction between the cavity wall and fractures will cause increased displacements and stresses in the rock in a complex manner. Thus, a thorough understanding of the dynamic response of fractures intersecting the excavation to incoming waves at various frequency ranges is important for the excavation's safety, including preventing rock falls and keeping the excavation stable and usable.

The dynamic response of cavities (e. g. Achenbach et al., 1984) and fractures (e. g. Yi et al., 1998) has been studied extensively but separately in seismic literature. To the author's best knowledge, no quality models currently exist to predict the dynamic response of an excavation in a fractured host medium to an incoming blast or seismic wave. The static analysis of the combined response of fractured tunnels has already been reported in the literature (Gupta, 1994). However, the reduction of the stiffness and integrity of the excavation due to fractures is far more significant under dynamic loads than static loads. In addition, upon certain incident waves, the cavity acts as a waveguide, either longitudinally or circumferentially, or both (Nagy *et al.*, 1994). It should be noted that guided waves are usually stronger and less attenuated than bulk waves. The presence of a longitudinal fracture plays an important role in the properties of the guided waves, especially in the circumferential direction.

In this study, we implemented a computational method to predict the dynamic response

of excavations in longitudinally fractured rock mass to seismic and blast waves. The fracture is represented by a widely used slip model, which has been extensively analyzed and verified by experiments in the literature (Schoenberg, 1980; Schoenberg & Sayers, 1995; Pyrak-Nolte & Cook, 1987; Pyrak-Nolte *et al.*, 1990, 1993). Displacements and stresses along and around the surfaces of the fracture and cavity were predicted in terms of the material properties of the rock, tunnel shape, fracture stiffness, fracture orientation, frequency and angle of the incident wave. Interesting simulation results were obtained.

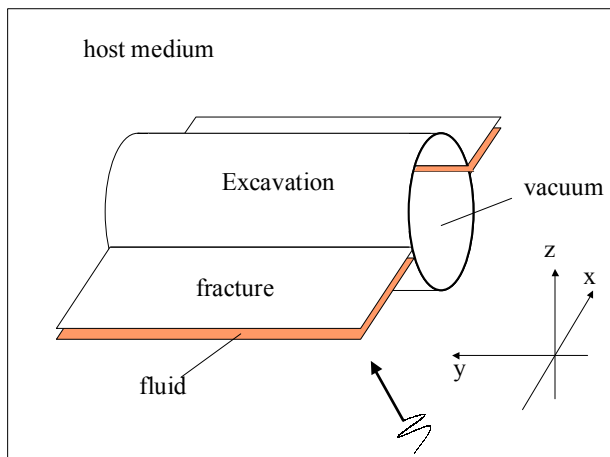


Figure 1 Geometry of a fractured tunnel impinged by a plane wave.

## 2. STATEMENT OF THE PROBLEM

Consider an excavation (Fig. 1) with an infinite extent in  $y$  and a constant cross section in the  $xz$  plane, embedded in an unbounded elastic medium. The interior of the excavation is filled with air. The host medium is uniform and isotropic except for a fracture or fractures intersecting the tunnel. The fracture is filled with fluid (air or water), and has infinite extent in  $y$  and  $x$ . The dynamic excitation is assumed to be a plane wave in the form of  $\exp[i\omega(x \cos\theta_x + y \cos\theta_y + z \cos\theta_z)/V - i\omega t]$ , where  $V$  is the wave speed (P or S),  $\theta_x$ ,  $\theta_y$ , and  $\theta_z$  are the angle of the incident ray with  $x$ ,  $y$ ,  $z$  axes, respectively. It is also assumed that the  $y$  dependence factor of  $\exp(i\omega y \cos\theta_y/V)$  can be separated from the  $x$ ,  $z$

dependence in all field quantities. As a result, the original problem is reduced to two dimensional, P-SV and SH problems. This paper considers the P-SV case only.

## 3. THE BIE METHOD

We have adopted a boundary integration equation approach. In the BIE method, only the boundaries of the cross section of the excavation and the fracture are discretized. Although the resulting matrix is not banded or symmetric, its size is several orders of magnitude smaller than that in the finite element method (FEM). Another advantage of the BIE method is its efficiency in solving problems involving a larger number of source-detector configurations. In this case, the total computational cost is merely slightly higher than that for a single source-detector pair. Furthermore, in the BIE model, the host medium surrounding the excavation and fracture is unbounded. Therefore radiation conditions at infinity are automatically satisfied, in contrast to the artificial radiation conditions imposed in the finite difference method (FDM) and FEM. Finally, certain frequency dependent properties, such as viscoelasticity, poroelasticity and permeability are of interest. FDM is incapable or inefficient in these aspects.

The standard form of BIE can be found in Bonnet (1995). In our model, the surface of the excavation is traction free. If we further assume that the surface of the fracture is also free, then the BIE, after discretization, can be reduced to linear equations of the form

$$\left( \left[ \frac{1}{2} I \right] + [f] \right) \{u\} = \{u_0\} \quad (1)$$

where  $[I]$  is the unit matrix,  $[f]$  is the matrix form of the coefficients of  $u$  in the BIE, which are associated with the stresses of the Green's functions between boundary nodes. Here we have used  $\{u\}$  and  $\{u_0\}$  to denote the vectors representing the unknown nodal displacements and the nodal displacements in the absence of the tunnel, respectively. Since  $[f]$  and  $\{u_0\}$  are given, the unknown displacement vector,  $\{u\}$ , can be

obtained through the use of a linear equation solver.

The BIE solution gives the boundary displacements directly, and the internal displacements through direct numerical integration. The hoop stress and stresses in the field can be obtained as well in a quite straightforward manner.

It should be noted that the slip model of fracture allows stresses across the fracture. Therefore, Eq. (1) is not valid unless appropriate modifications are made. The following section and the Appendix will address this issue.

#### 4. THE SLIP MODEL OF THE FRACTURE

This slip model in this study follows the work of Schoenberg (1980), where an infinite planar fracture is considered as an interface with the following boundary conditions

$$\begin{aligned}
 \sigma_n^+ &= \sigma_n^- = \sigma_n \\
 \sigma_s^+ &= \sigma_s^- = \sigma_s \\
 u_n^+ - u_n^- &= \frac{\sigma_n}{K_n} \\
 u_s^+ - u_s^- &= \frac{\sigma_s}{K_s}
 \end{aligned} \tag{2}$$

where + and - denote opposite sides of the fracture interface,  $\sigma$  is stress,  $u$  is displacement, and subscripts  $n$  and  $s$  denote normal and shear directions respectively. These conditions correspond to continuity of normal and shear stress across the interface, and discontinuity of displacement across the interface. The parameters  $K_n$  and  $K_s$  are the normal and shear stiffnesses of the fracture, respectively.

When applying the slip model to BIE, there are two major considerations. It has been assumed that the fracture's thickness is negligible. Therefore, we must first avoid the singularity of the Green's functions and associated stresses, which form the coefficients of the BIE. Further, we should be able to express the unknown stresses at the interface nodes in terms of their displacements and reduce the number of unknowns along the interface to its  $\frac{1}{2}$ .

Figure 2 shows the concept of the slip model used in our BIE approach. Boundary nodes are placed apart on the two sides of the slip line. Each pair of opposite nodes is interconnected by

a spring to support tension and shear forces. The basic unknowns at the nodes are the nodal displacements only, similar to the traction free nodes. The stress across the interface is proportional to the strain between the opposite nodes. The normal or shear stiffness of the spring,  $K_1$  or  $K_2$ , is dependent upon: i) the stiffness of the elastic solid within the distance between adjacent nodes,  $(\lambda+2\mu)/h$  or  $\mu/h$ ; and ii) the stiffness of the slip interface,  $K_n$  or  $K_s$ , such that

$$\begin{aligned}
 \frac{1}{K_1} &= \frac{h}{\lambda + 2\mu} + \frac{1}{K_n} \\
 \frac{1}{K_2} &= \frac{h}{\mu} + \frac{1}{K_s}
 \end{aligned} \tag{3}$$

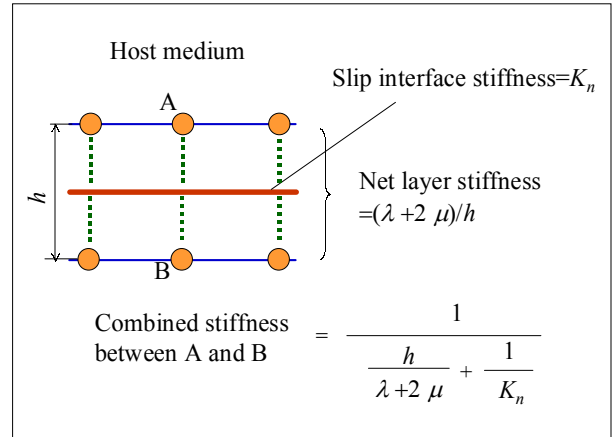


Figure 2 A slip model for the boundary integral equation method.

Detailed analysis of this model and its implementation in our BIE approach is given in the Appendix. The result of the analysis leads the discretized BIE to Eq. (A5), which is similar to Eq. (1), but with an additional term in the left hand matrix, accounting for the stresses between opposite interfacial nodes. The analysis considers two opposite nodes only. We have extended Eq. (A5) to the entire interface and ignored the interactions between non-opposite nodes.

We would like to point out that when  $h$  is small compared to the wavelength and dimension of the tunnel, the influence of its variation on the result is negligible.

In the results presented below, we have introduced the normalized slip stiffness,  $\kappa_n$  and  $\kappa_s$ , as follows

$$\begin{aligned}\kappa_n &= \frac{K_n l}{\lambda + 2\mu} \\ \kappa_s &= \frac{K_s l}{\mu}\end{aligned}\quad (4)$$

where  $\lambda$  and  $\mu$  are the elastic constants of the host medium, and  $l$  is the wavelength. Clearly, when  $\kappa_n$  and  $\kappa_s$  are infinity, the interface becomes rigid and the medium is uniform; when  $\kappa_n$  and  $\kappa_s$  vanish, the interface is replaced by two traction free, separate surfaces.

## 5. NUMERICAL RESULTS

The numerical results are focused on the effect of frequency dependent normalized slip stiffnesses,  $\kappa_n$  and  $\kappa_s$ , on the dynamic response of a dome shaped cavity with a slip type fracture, in comparison with one with no fracture, and one with a surface traction free fracture.

Our algorithm is not limited to any ranges of frequency and is therefore can be used to study the response of an excavation to waves in seismic, blast, rock burst and other excitations. For illustration purposes, the example below assumes that the frequency of the incoming wave is 0.25 kHz. The P wave and S wave speeds in the host medium are 1.175 km/sec and 1 km/sec, respectively. The mass density is 1 gm/cm<sup>3</sup>. The height and the width of the dome are 5 m and 3 m, respectively. A horizontal fracture is intersecting the cavity at a height of 3 m. The distance between opposite nodes along the fracture interface,  $h$ , is 0.25 m. Normalized slip stiffness  $\kappa_n$  and  $\kappa_s$  range from 0 to  $\infty$ . In all cases, we assume that  $\kappa_n = \kappa_s$ . The hoop stress has been normalized to the amplitude of the maximum stress of the incident wave. In plots of boundary hoop stress, the baseline represents both the physical boundary of the cavity and the numeric position of zero stress, while outward and inward portions of the curves denote tensile and compression stresses, respectively.

Figures. 3 and 4 show the hoop stress on the boundary of the cavity. When the P wave incidence is normal (Fig. 3), the degree of stress

concentration is increased roughly in the following order:  $\kappa_n, \kappa_s = \infty, 2, 0, 6, 400, 200, 16$ . In Figure 4, the incidence angle is 45° from below, and the above order is slightly modified as  $\kappa_n, \kappa_s = \infty, 0, 2, 400, 200, 6, 16$ . Note that some of these curves are not shown in Figures. 3 and 4 due to limited space.

Next, we study the effect of the normalized slip stiffness on the stress distribution in the surrounding area of the cavity. Figures. 5-7 show the quiver (vector field) plots of real part of the principal stresses for three cases: i) no fracture; ii) traction free fracture; and iii) a fracture with  $\kappa_n = \kappa_s = 6$ . It can be seen that the stress field for a cavity with a free fracture is more drastic and complex than that with no fracture, and this pattern is even more intensified when the slip interface has a moderate value of the normalized lip stiffnesses, especially near the fracture.

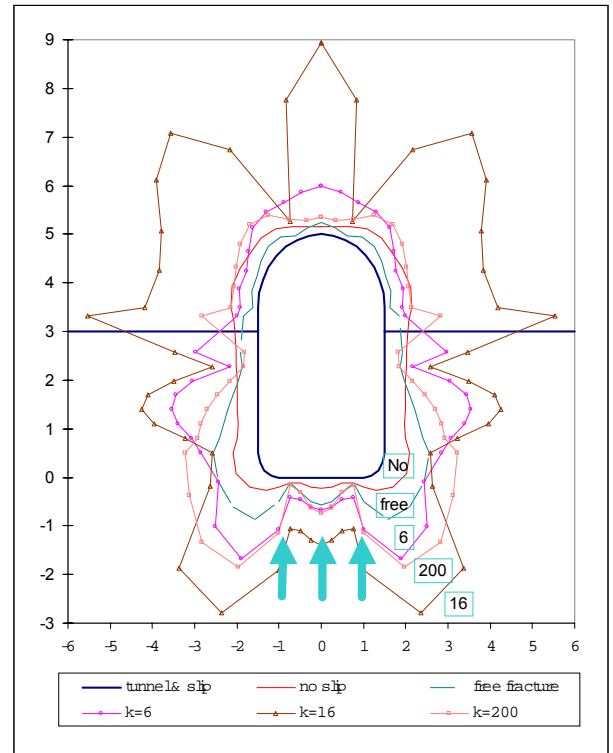


Figure 3 Hoop stress due to an upgoing P wave for various values of normalized slip stiffness.

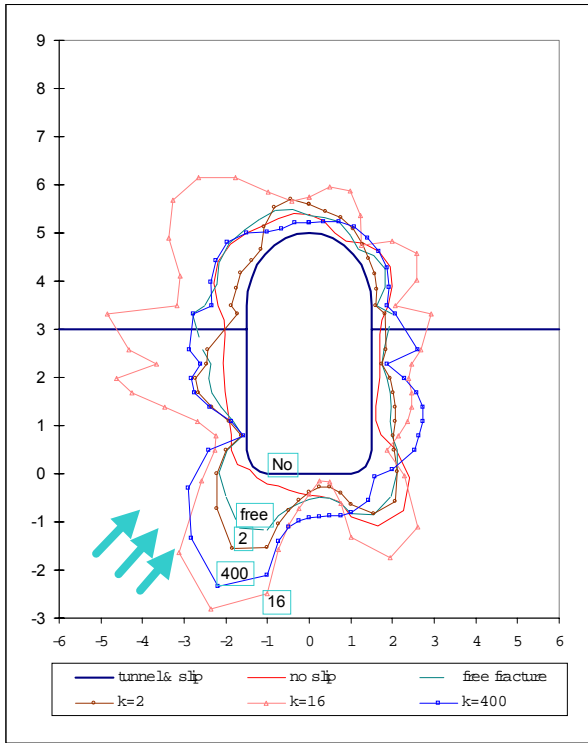


Figure 4 Hoop stress due to a 45° P wave for various values of normalized slip stiffness.

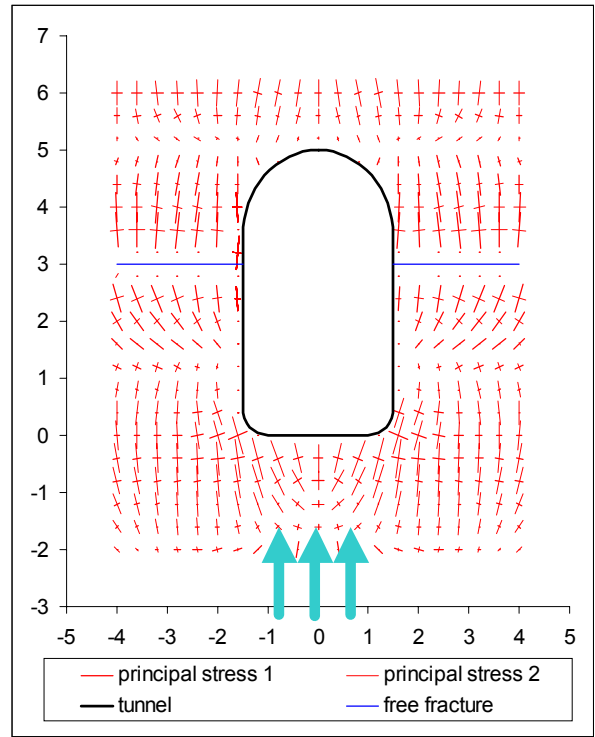


Figure 6 Principal stresses surrounding a tunnel with a free fracture

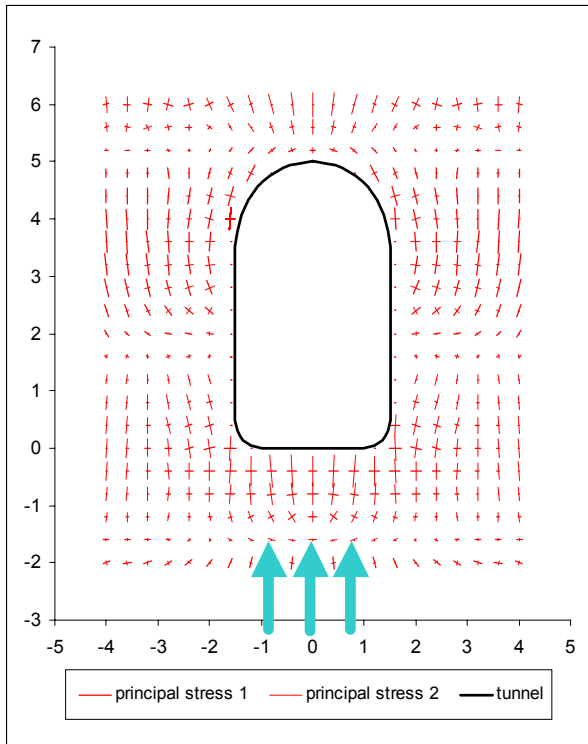


Figure 5 Principal stresses surrounding a tunnel with no fracture.

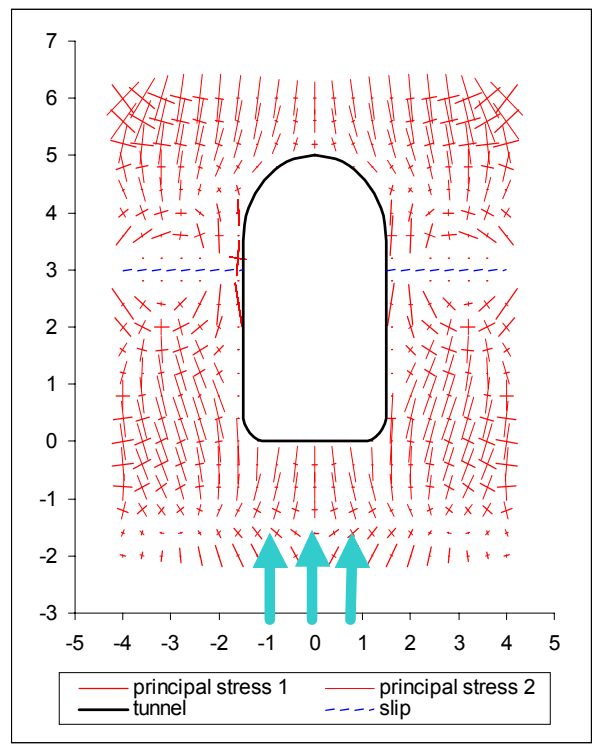


Figure 7 Principal stresses surrounding a tunnel with a slip interface

## 6. CONCLUSIONS

A BIE technique is developed to include the slip model of fracture and study the dynamic response of a fractured underground excavation to incoming waves. A robust computer algorithm based on this technique has been implemented and tested. This algorithm predicts displacement and stress fields for typical shapes of excavations, arbitrarily oriented fracture(s) with any value of slip stiffness, for a wide range of frequencies.

Preliminary parametric studies show that an intersecting fracture re-distributes and usually amplifies the stress along and around the surface of the cavity. For certain combinations of the above parameters, the stress amplification and complication can be very significant. It is found that the strongest stress concentration and deformation do not occur when the traction on the fracture is free but occur when the normalized slip stiffnesses are of a moderate value. Therefore, it is essential to evaluate the slip stiffnesses of the fracture and carry out reliable analysis of the behavior of the fractured excavation during dynamic events. In this regard, this paper provides a useful tool.

## ACKNOWLEDGEMENTS

Principal support for this work was provided by Southwest Research Institute Internal Research Program. The assistance and advisory guidance provided by Dr. A. Ghosh, Center for Nuclear Waste Regulatory Analyses is gratefully acknowledged and appreciated.

## REFERENCES

- Achenbach, J. D., Angel, Y.C. & Lin, W., 1984, Scattering from surface-breaking and near surface cracks, in G.C. Johnson (Ed.), *Wave propagation in homogeneous media and ultrasonic nondestructive evaluation*, ASME AMD-62: 93-109.
- Bonnet, M., 1999, *Boundary integral equation method for solids and fluids*, John Wiley & Sons Ltd.
- Gupta, N. K., 1994, Flaw acceptance criteria for Transuranic (TRU) waste drums, in *Fracture mechanics applications*, ASME PVP-287.

- Hornby, B. E., Johnson, D. L., Winkler, K. W., & Plumb, R. A., 1989, Fracture evaluation using reflected Stoneley-wave arrivals, *Geophysics* 54(10): 1274-1288.
- Nagy, P. B., Blodgett, M. & Golis, M., 1994, Weep hole inspection by circumferential creeping waves, *NDT & E International* 27: 131-142.
- Pyrak-Notle, L. J., Myer, L. R. & Cook, N. G. W., 1990, Transmission of seismic waves across single natural fractures, *J. Geoph. Res.* 95(B6): 8617-8638.
- Pyrak-Notle, L. J., Xu, J. & Haley, G. M., 1993, Elastic interface waves propagating in a fracture, *Phys. Rev. Lett.* 68(24): 3650-3653.
- Schoenberg, M., 1980, Elastic wave behavior across linear slip interfaces, *J. Acoust. Soc. Am.*: 68(5): 1516-1521.
- Schoenberg, M., & Sayers, C. M., 1995, Seismic anisotropy of fractured rock, *Geophysics* 60: 204-211.
- Yi, W., Nakagawa, S., Nihei, K. T., Rector, J. W., Myer, L. M., & Cook, N. G. W., 1998, Numerical investigation of fracture channel waves, *Expanded Abstracts of the 68<sup>th</sup> SEG Annual Meeting*.

## APPENDIX: Analysis of the slip model in BIE

Let A and B be a pair of nodes, distanced by  $h$ , which is small compared to the wavelength, in an unbounded medium (Fig. 2). Then the discretized BIE involves four unknowns:

$$\left[ \frac{1}{2}I + f \right] \begin{Bmatrix} u_A \\ u_B \end{Bmatrix} + [g] \begin{Bmatrix} \sigma_A \\ \sigma_B \end{Bmatrix} = \begin{Bmatrix} u_A^0 \\ u_B^0 \end{Bmatrix} \quad (\text{A1})$$

and

$$\left[ \frac{1}{2}I - F \right] \begin{Bmatrix} u_A \\ u_B \end{Bmatrix} - [G] \begin{Bmatrix} \sigma_A \\ \sigma_B \end{Bmatrix} = \begin{Bmatrix} 0 \\ 0 \end{Bmatrix} \quad (\text{A2})$$

Among the notations used in the above, superscript 0 is associated with the incident field, upper-cased letters denote the area between the opposite nodes, and lower-cased letters denote the rest of the host medium. For example,  $[g]$  is the matrix form of the coefficients of the unknown stresses, obtained from the Green's functions regarding two distinct boundary nodes, and  $[f]$  is the matrix form of the coefficients of the unknown displacements, obtained from the stresses associated with these Green's functions.

We now insert a slip interface between A and B. Let  $\eta_{\text{slip}}$  be a normalized stiffness, which is defined as the ratio of  $K_n$  or  $K_s$  divided by a unit

stiffness. For convenience, we take this unit stiffness as that of the host medium with a thickness  $h$ . Assume that

$$\sigma_A = \sigma_B = k(u_B - u_A) \quad (\text{A3})$$

where  $u_A$  and  $u_B$  have been normalized to  $h$  and  $k$  is defined as

$$\frac{1}{k} = \frac{h}{\lambda + 2\mu} \left(1 + \frac{1}{\eta_{slip}}\right) \quad (\text{A4})$$

Consequently, Eq. (A3) yields

$$\left[ \frac{1}{2}I + f \right] \begin{Bmatrix} u_A \\ u_B \end{Bmatrix} + [g] \begin{Bmatrix} k(u_B - u_A) \\ k(u_B - u_A) \end{Bmatrix} = \begin{Bmatrix} u_A^0 \\ u_B^0 \end{Bmatrix} \quad (\text{A5})$$

Note that the number of unknowns has been reduced to two, and stresses are not explicitly present in the expression.

Let us examine two special cases.

(1) Case 1 (weak slip interface)

When  $\eta_{slip}$  is much smaller than 1, we have

$$k \approx \eta_{slip} \frac{\lambda + 2\mu}{h} \ll \frac{\lambda + 2\mu}{h} \quad (\text{A6})$$

which leads to

$$\left[ \frac{1}{2}I + f \mp kg \right] \begin{Bmatrix} u_A \\ u_B \end{Bmatrix} = \begin{Bmatrix} u_A^0 \\ u_B^0 \end{Bmatrix} \quad (\text{A7})$$

When  $k=0$ , this model is reduced to the case with a free surface, Eq. (1) in the main text.

(2) Case 2 (strong slip interface)

When  $\eta_{slip}$  is much greater than 1, we have

$$k \approx \frac{\lambda + 2\mu}{h} \quad (\text{A8})$$

Define the change of rigidity due to the slip as follows.

$$k' = \frac{\lambda + 2\mu}{h} - k = \frac{\lambda + 2\mu}{(1 + \eta_{slip})h} \ll \frac{\lambda + 2\mu}{h} \quad (\text{A9})$$

Then after some algebra, Eq. (A7) can be written as

$$\left[ \frac{1}{2}I + f \mp k'g \right] \begin{Bmatrix} u_A \\ u_B \end{Bmatrix} = \left[ \frac{1}{2}I + f \mp k'g \right] \begin{Bmatrix} u_A^0 \\ u_B^0 \end{Bmatrix} \quad (\text{A10})$$

Note that  $k$  or  $k'$  must be sufficiently small to permit a reliable solution of the weak or strong slip model, respectively.